

# Journal of Materials Chemistry A

Accepted Manuscript



This is an *Accepted Manuscript*, which has been through the Royal Society of Chemistry peer review process and has been accepted for publication.

*Accepted Manuscripts* are published online shortly after acceptance, before technical editing, formatting and proof reading. Using this free service, authors can make their results available to the community, in citable form, before we publish the edited article. We will replace this *Accepted Manuscript* with the edited and formatted *Advance Article* as soon as it is available.

You can find more information about *Accepted Manuscripts* in the [Information for Authors](#).

Please note that technical editing may introduce minor changes to the text and/or graphics, which may alter content. The journal's standard [Terms & Conditions](#) and the [Ethical guidelines](#) still apply. In no event shall the Royal Society of Chemistry be held responsible for any errors or omissions in this *Accepted Manuscript* or any consequences arising from the use of any information it contains.



## Journal Name

## ARTICLE

Received 00th January  
20xx,  
Accepted 00th January  
20xx  
DOI: 10.1039/x0xx00000x

[www.rsc.org/](http://www.rsc.org/)

## Update on anode materials for Na-ion batteries

Hongyan Kang, Yongchang Liu, Kangzhe Cao, Yan Zhao, Lifang Jiao\*, Yijing Wang and Huatang Yuan  
Na-ion batteries have sprung up in recent years, due to their advantages of the natural abundance, low cost and environmental friendliness. In this article, we review the up-to-date research progress on anode materials for Na-ion batteries from five respects: carbon-based materials, alloy-based materials, metal oxides and sulfides based on conversion reaction, titanium-based compounds with insertion mechanism, and organic composites. In particular, we not only summarize the Na-storage mechanism of these anodes, but also discuss the failure mechanism. The problems and challenges associated with these anodes are pointed out. Furthermore, on the basis of extensive literatures and our experimental works, the feasible strategies are suggested for designing high performance anode materials. After further in-depth exploration and investigation, we believe that Na-ion batteries are promising alternative to lithium-ion batteries for low cost and large-scale energy storage system in near future.

### 1 Introduction

Energy is an essential material basis for human survival and development. With the rapid exhaustion of non-renewable fossil fuels and aggravation of environment problems, the development of renewable and clean energy such as, wind, solar, biomass, tide and geothermal is becoming more and more important. So, a large-scale energy storage system (ESS) becomes extremely necessary to modulate intermittent renewable resources and integrate them into the grid safely and smoothly.<sup>1-4</sup>

Lithium-ion batteries (LIBs) have developed rapidly and controlled the market of second battery industry since their first

commercialization in 1991. They have been widely applied in portable electrical devices.<sup>5</sup> However, large-scale application of LIBs suffers from challenges due to the scarcity, maldistribution and high cost of lithium resources. As shown in Table 1,<sup>6,7</sup> compared with lithium, sodium has the advantages of the natural abundance and low cost. Moreover, sodium and lithium are in the same main group, showing similar chemical properties. Therefore, Na-ion batteries (NIBs) are recognized to be the most promising alternative to LIBs for achieving large-scale ESS and sustainable application.<sup>8-11</sup>

Room temperature stationary Na-ion batteries started to be studied before 1980 in parallel to LIBs. However, the usable energy density of Na system is believed to be much lower than that of Li system. Moreover, available negative electrodes had not been found for a long period of time. For example, graphite,<sup>12</sup> the conventional anode for LIBs, fails to intercalate sodium effectively, due to the mismatching of interlayer distance of graphite to the larger Na<sup>+</sup> radius. Si-based material is expected as the most promising anode for LIBs but not in NIBs systems.<sup>13</sup> This is because Si cannot incorporate Na<sup>+</sup> ions like in case of Li<sup>+</sup> ions. The two

Key Laboratory of Advanced Energy Materials Chemistry (MOE), Collaborative Innovation Center of Chemical Science and Engineering (Tianjin), College of Chemistry, Nankai University, Tianjin 300071, PR China.  
E-mail: [jjiaolf@nankai.edu.cn](mailto:jjiaolf@nankai.edu.cn); Fax: +86 22 23504527; Tel: +86 22 23504527



Hongyan Kang received her B. Sc. degree in material chemistry in 2013 from Hebei University. Currently, she is a postgraduate researcher in the group of Assoc. Prof. Lifang Jiao at Nankai University. Her research interests are in advanced materials for Na-ion batteries.



Lifang Jiao is an Associate Professor at Nankai University, China. She received her BS and MS degree in chemistry from Hebei Normal University (China) in 1999 and 2002, respectively, and PhD degree from Nankai University (China) in 2005. She has been working as a senior research fellow in Shixue Dou's group at University of Wollongong (Australia) in 2014. Her research interests include energy conversion and storage (secondary batteries including lithium, sodium, magnesium, and supercapacitors), hydrogen storage materials and electrocatalytic hydrogen evolution.



Hard carbon, so called non-graphitic carbon, has been widely used as anodes for NIBs,<sup>25-28</sup> owing to its highly disordered structure and large interlayer distance. The structure of hard carbon is composed of carbon layers (graphene-like) and micropores. Fig. 2b shows the typical charge and discharge curves of hard carbon, which exhibits two distinct features: a sloping region and a long plateau region below 0.1 V which can be ascribed to the insertion of Na<sup>+</sup> between parallel layers and into nanopores of hard carbon, respectively. This mechanism of the Na<sup>+</sup> insertion into hard carbons was initially studied in 2000 by wide angle *in situ* X-ray scattering<sup>16</sup> and further confirmed by solid state <sup>23</sup>Na NMR recently.<sup>29</sup> On the

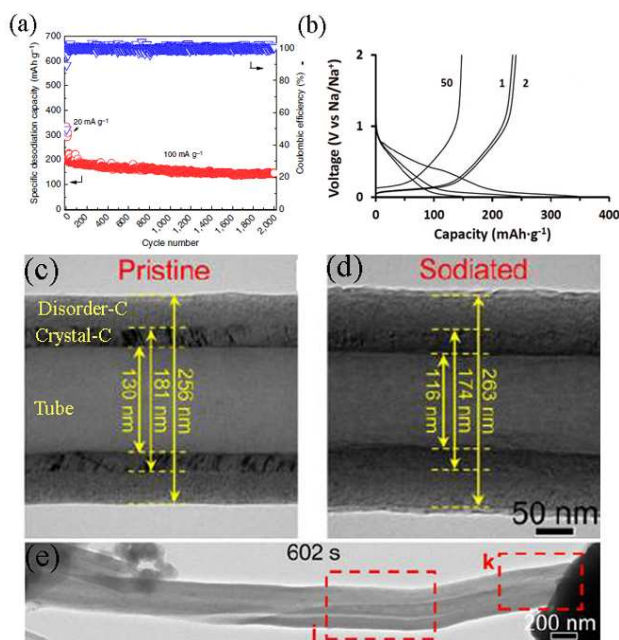


**Fig. 2** (a) cycling stability of expanded graphite at 100 mA g<sup>-1</sup> with activation at 20 mA g<sup>-1</sup> for the initial 10 cycles. (b) Charge/discharge curves of the selected cycles for hard carbon. The TEM images of (c) pristine carbon nanofibers, (d) sodiated carbon nanofibers, (e) sodiation-induced crack at 602 s. (a) reprinted with permission from Macmillan Publishers Ltd.: (*Nat. Commun.*) (ref. 20), copyright 2014. (b) reprinted with permission from ref. 25. Copyright 2014 The Electrochemical Society. (c, d, e) reprinted with permission from ref. 34. Copyright 2014 American Chemical Society.

whole, hard carbon exhibits a reversible capacity of 200-300 mA h g<sup>-1</sup> at the low current density. However, the high-rate capability is insufficient due to the low graphitization of hard carbon. It must also be noted that a large portion of capacity for hard carbon comes from low potential (ca. 0 V), close to the sodium electroplating potential, which may cause serious safety hazard in fast charging process.

There are mainly three effective strategies to ameliorate the unsatisfactory cyclic stability and rate capability of carbon materials. Firstly, prepare nanostructured carbon materials, which have the advantage of good conducting connective and structural stability. For example, carbon nanosheets, as thin as 60 nm, derived from biomass precursor (peat moss) have been reported.<sup>30</sup> The carbon could form highly ordered pseudographitic arrays with a substantially dilated interlayer spacing (0.388 nm). By incorporating a mild air activation step, micro- and mesoporosity were introduced, which can tremendously improve the rate performance. The optimized structures achieved a high capacity of 255 mA h g<sup>-1</sup> at 100 mA g<sup>-1</sup> after 210 cycles, with nearly 100% coulombic efficiency. The outstanding performance and the economical, environment friendly synthesis may make carbonized peat moss a potential anode for NIBs.

Secondly, design hollow structure. Hollow carbon nanospheres showed much better rate performance compared to its solid spheres.<sup>31</sup> Cao and co-workers reported the hollow carbon nanowires derived from hollow polyaniline, with an initial capacity of 251 mA h g<sup>-1</sup> and 82 % capacity retention after 400 cycles at 50 mA h g<sup>-1</sup>.<sup>32</sup> The achieved good properties benefited from the unique hollow structure, which not only offered a buffering zone to effectively release the mechanical stress caused by Na<sup>+</sup> insertion/extraction, but also shortened the Na<sup>+</sup> diffusion path to boost mass transport.

Finally, heteroatom doping in carbon structure is also an efficient way. Wang *et al.* prepared N-doped interconnected carbon nanofibers by direct pyrolyzation of PPy nanofiber webs, reaching a high capacity of 73 mA h g<sup>-1</sup> at an extremely high rate of 20 A g<sup>-1</sup> between 0.01-2.0 V.<sup>33</sup>

In order to explore the mechanical degradation and microstructure evolution of carbon-based anodes during sodiation, Wang's group studied the electrochemical sodiation of hollow carbon nanofibers (CNFs) by *in situ* TEM.<sup>34</sup> The hollow CNFs were

**Table 2** Properties of carbon-based materials

Carbon materials	Electronic Conductivity (S cm <sup>-1</sup> ) <sup>a</sup>	Interlayer Distance (nm)	Voltage (V versus Na <sup>+</sup> /Na)	S <sub>BET</sub> (m <sup>2</sup> g <sup>-1</sup> )	mechanism
Expanded graphite <sup>20</sup>	100	0.43	0-0.3, 0.3-2	30-34	insertion
Graphene <sup>21</sup>	10 <sup>3</sup> -10 <sup>6</sup>	0.365-0.371	0.01-2	330.9	adsorption
Hard carbon	10-100	0.39 <sup>28</sup>	0.1, 0.1-1.2	1272 <sup>26</sup>	insertion between parallel layers and into nanopores
Nanosheets <sup>30</sup>	10-100	0.388	0.2, 0.2-1.2	196.6	insertion between graphene layers (mainly)
Hollow carbon nanospheres <sup>31</sup>	10-100	0.401	0-1.5	410	insertion between graphene layers (mainly)
N-doped nanofibers <sup>33</sup>	--	0.369	0.01-1.5	81.7	surface adsorption and redox reactions

<sup>a</sup> the data of electronic conductivity are not from the corresponding refs. 20, 21, 30, 31.



## Journal Name

## ARTICLE

composed of a bilayer wall with an outer layer of disordered carbon (d-C) and an inner layer of crystalline carbon (c-C) (Fig. 2c). During sodiation, the flexible d-C showed approximately three times volume expansion of c-C (Fig. 2d), indicating a higher Na storage capacity in d-C than c-C. It was also found that the mechanical degradation of hollow CNFs was ascribed to the frequent formation of longitudinal cracks close to the c-C/d-C interface after sodiation (Fig. 2e). The geometrical changes of the hollow CNFs were due to the anisotropic sodiation strains in c-C and d-C.

### 3 Alloy-based materials

Alloy-based materials have been proved to be promising anode electrodes owing to their high theoretical capacity (as shown in Fig. 3). They can alloy with sodium to form rich alloy phases, yielding a much higher capacity than carbon-based materials. For LIBs, Si is the most studied alloy materials due to its ultra high theoretical specific capacity of 4200 mA h g<sup>-1</sup>, however, it is indeedly Na inactive. Indium (In) is also explored as anode for NIBs, however, it just exhibits a low capacity of ca. 100 mA h g<sup>-1</sup>.<sup>35</sup> Therefore, this section pays attention to the extensively studied the elements in group 14 (Sn, Ge) and group 15 (P, Sb) owing to their excellent electrochemical performance, low cost and environmental friendliness. Some of their properties are listed in Table 3.

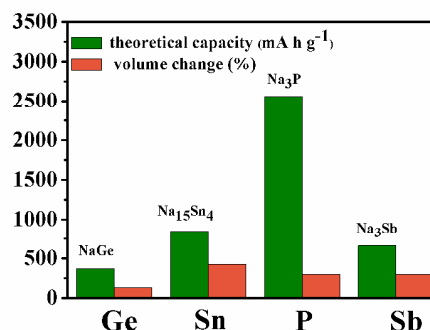


**Fig. 3** Theoretical gravimetric capacity and volume change of the Ge, Sn, P, and Sb elements

Ceder's group<sup>13</sup> reported that Na (de)insertion into the crystalline tin occurred in four steps, NaSn<sub>5</sub>, NaSn, Na<sub>3</sub>Sn and Na<sub>15</sub>Sn<sub>4</sub> (Fig. 4a). The final phase Na<sub>15</sub>Sn<sub>4</sub> after full sodiation in NIBs has been experimentally detected.<sup>36,37</sup> A high theoretical capacity of 847 mA h g<sup>-1</sup> can be achieved from Sn to Na<sub>15</sub>Sn<sub>4</sub>, with the huge volume expansion of 420%.

Antimony (Sb) is also a promising alloy anode for NIBs, with a high theoretical capacity of 660 mA h g<sup>-1</sup>. Darwiche *et al.* explored the reaction mechanism of pure micrometric Sb in NIBs by *in situ*

**Table 3** Summarization of alloying and conversion reaction-based materials

Mechanism	Materials	Electrical conductivity (S cm <sup>-1</sup> )	Theoretical capacity (mA h g <sup>-1</sup> )	Abundance in the earth crust (ppm)
<b>Alloying</b>				
$M + xNa^+ + xe^- \leftrightarrow Na_xM$	Sn	$9 \times 10^4$	847	2.2
	P	$10^{-14}$	2596	1000
	Ge	$\sim 10^{-2}$	369	1.8
	Sb	$2.5 \times 10^4$	660	0.2-0.5
<b>Conversion</b>				
$MO_x + 2xNa^+ + 2xe^- \leftrightarrow xNa_2O + M$	NiCo <sub>2</sub> O <sub>4</sub>	0.1-0.3	890	--
	Fe <sub>2</sub> O <sub>3</sub>	$7 \times 10^{-3}$	1007	41000
	CuO	0.03-1	674	100
	Co <sub>3</sub> O <sub>4</sub>	$3.1 \times 10^{-5}$	890	10
	MnO <sub>x</sub>	$10^{-4}$ - $10^{-6}$	700-1000	950
$MO_x + 2xNa^+ + 2xe^- \leftrightarrow xNa_2O + M$ $M + yNa^+ + ye^- \leftrightarrow Na_yM$	SnO <sub>2</sub>	$4.5 \times 10^{-5}$	782	2.2
	Sb <sub>2</sub> O <sub>3</sub>	--	1102	0.2-0.5
$MS_2 + xNa^+ + xe^- \rightarrow Na_xMS_2$ (Intercalation) $Na_xMS_2 + (4-x)Na^+ + (4-x)e^- \rightarrow M + 2Na_2S$ (Conversion)	MoS <sub>2</sub>	$3.3 \times 10^{-7}$ (bulk)	670	1.5
	SnS <sub>2</sub>	$2 \times 10^{-3}$	584	2.2
	FeS <sub>2</sub>	0.06-5	893	41000

XRD.<sup>38</sup> It was revealed that Na inserted into crystalline Sb to form intermediate phases  $\text{Na}_x\text{Sb}$ , which were mostly amorphous and further to form hexagonal  $\text{Na}_3\text{Sb}$  as a final product. However, during the charge/discharge process, Na alloys with Sb accompanying with a large volume change of 293%, resulting in the poor cyclability at high current density.

Germanium (Ge) can alloy with Na to form NaGe calculated by Ceder's group<sup>13</sup>, delivering a theoretical capacity of  $369 \text{ mA h g}^{-1}$ . And it was first reported as anode material for NIBs by Baggetto.<sup>39</sup> However, the application of Ge is held back by its sluggish kinetics and poor cyclability.

Phosphorus (P) has three allotropes: white, black, and red phosphorus. Among these allotropes, red phosphorus is relatively stable, commercially available and most studied as anode for NIBs. P provides a highest theoretical capacity of  $2596 \text{ mA h g}^{-1}$  ( $\text{Na}_3\text{P}$ ) and appropriate redox potential of about  $0.4 \text{ V vs. Na}^+/\text{Na}$ .<sup>40,41</sup> However, just as other alloy based materials, P also undergoes large volume expansion and serious electrolyte decomposition. In addition, P has a quite low electrical conductivity ( $1 \times 10^{-14} \text{ S cm}^{-1}$ ).

As noted above, the main challenge for alloy-based materials is the enormous volume expansion (Fig. 3), which will result in continuous pulverization of these electrode materials and then a steep deterioration of electrochemical performance. In recent years, much research effort has been devoted to reducing the negative effect of volume change and boosting the electronic conduction, and several approaches have been proposed.

The first critical approach is to prepare unique nanostructures, which can better accommodate the stress and strain without pulverizing, and reduce the ionic and electronic transport pathways. For example, Nam *et al.*<sup>42</sup> reported bare Sn nanofibers using Triton X-100 as inducer by simple electrodeposition. As electrode materials for NIBs, the Sn nanofibers exhibited good cyclic stability, with an initial capacity of  $816.37 \text{ mA h g}^{-1}$  and 95% capacity retention after 100 cycles at  $0.1 \text{ C}$ . However, the coulombic efficiency and rate capability needed to be further improved. Meng *et al.* prepared monodisperse Sb nanocrystals (10–20 nm), which exhibited improved rate capability and cycling stability with respect to microcrystalline Sb.<sup>43</sup> Abel *et al.* compared the electrochemical performance of nanocolumnar and dense Ge thin films.<sup>44</sup> The initial capacity of the nanocolumnar films was  $430 \text{ mA h g}^{-1}$  and 88% capacity was maintained over 100 cycles at  $\text{C}/5$ , while the dense films started to decay after 15 cycles.

The second efficient approach is to introduce carbon to the system, in which metal particles can be coated with carbon or embedded in carbon matrix. In this system, carbon matrix can act as a buffer to suppress the volume change and particle aggregation of the metal during sodiation/desodiation process, thus addressing the major challenges of loss of electrical contact, pulverization and low utilization rate associated with alloy anode. In addition, carbon phase can also boost the electrical conductivity of the electrodes. A series of  $\text{Sn}/\text{C}$ <sup>37,45,46</sup>,  $\text{Sb}/\text{C}$ <sup>47–51</sup> and  $\text{P}/\text{C}$ <sup>40,41,52–54</sup> composites have been synthesized with markedly enhanced electrochemistry performance.

Our group synthesized Sn@carbon composite with ultrasmall Sn nanoparticles ( $\sim 8 \text{ nm}$ ) homogeneously embedded in spherical carbon (8-Sn@C) network (Fig. 4b) using an aerosol spray pyrolysis method.<sup>37</sup> When used as anode for NIBs, the 8-Sn@C electrode

showed a high reversible capacity of  $493.6 \text{ mA h g}^{-1}$  at  $200 \text{ mA g}^{-1}$ . Moreover, the capacity of  $349 \text{ mA h g}^{-1}$  even at high rate of  $4 \text{ A g}^{-1}$  and  $445 \text{ mA h g}^{-1}$  after 200 cycles with negligible fading at  $500 \text{ mA g}^{-1}$  were achieved (Fig. 4d). The high-rate capability and remarkable cycling stability of 8-Sn@C benefited from synergetic effects between the well-dispersed ultrasmall Sn nanoparticles and the conductive carbon network as stated above.

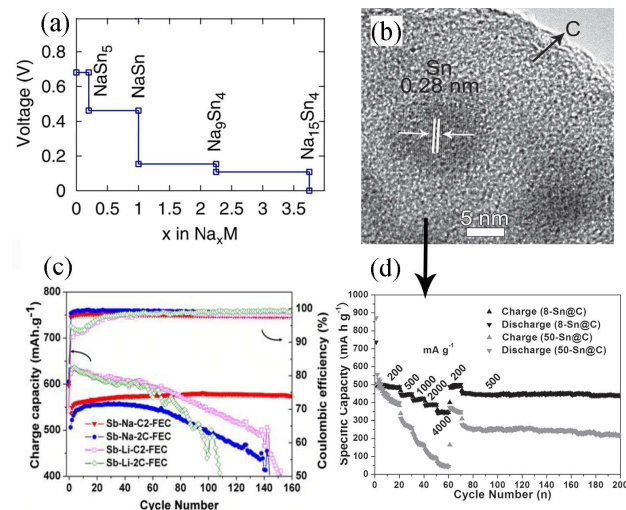


**Fig. 4** (a) Na-Sn voltage curves calculated using DFT (b) HRTEM images of 8-Sn@C. (d) Rate capability and cycling performance of the 8-Sn@C and 50-Sn@C electrodes. (c) Cycling performance of Sb electrode vs.  $\text{Na}^+$  and  $\text{Li}^+$  at  $\text{C}/2$  with addition of 5% FEC. (a) reprinted with permission from ref. 13. Copyright 2011 The Electrochemical Society. (b, d) reprinted with permission from ref. 37. Copyright 2014 Wiley-VCH Verlag GmbH & Co. KGaA, Weinheim. (c) reprinted with permission from ref. 38. Copyright 2012 American Chemical Society.

Sb/C nanofibers were prepared by electrospinning and subsequent calcinations.<sup>50</sup> The Sb nanoparticles with 15–20 nm diameters were uniformly dispersed in carbon nanofibers. It exhibited a high capacity of  $631 \text{ mA h g}^{-1}$  at the rate of  $40 \text{ mA g}^{-1}$  and  $337 \text{ mA h g}^{-1}$  at a high rate of  $3000 \text{ mA g}^{-1}$ . It is worth mentioning that electrospinning technique and above mentioned aerosol spray pyrolysis method are effective ways to prepare M/C composites owing to their simplicity, low cost and easy large-scale production.

Qian *et al.*<sup>40</sup> and Kim *et al.*<sup>41</sup> reported amorphous P/carbon composites through high-energy ball-milling, which delivered a high reversible capacity of  $1750 \text{ mA h g}^{-1}$  at  $250 \text{ mA g}^{-1}$  after 40 cycles and  $1890 \text{ mA h g}^{-1}$  at  $143 \text{ mA g}^{-1}$  for 30 cycles, respectively. Very recently, single-walled carbon nanotube (SWCNT) and graphene nanosheets were utilized as the conducting matrix to improve electrical conductivity of red phosphorus and alleviate the volume change during sodiation/desodiation process.<sup>52,53</sup> Moreover, an black (orthorhombic) phosphorus/carbon composite was also prepared, with an initial capacity of approximately  $1300 \text{ mA h g}^{-1}$ . The lower capacity was attributed to the incomplete transformation to  $\text{Na}_3\text{P}$  demonstrated by XRD.<sup>54</sup>

The third promising strategy is to design M-(Sn, Sb, P, Ge) intermetallics, where M is an electrochemically inactive component.

In this approach, the intermetallics can convert to M/Sn composite in the first cycle. The M acts as an electrochemically inactive matrix to alleviate volume changes during sodiation/desodiation. This introduced phase can also improve the electric conductivity of the system. And numerous M-Sn (M= Cu, Ni and Co),<sup>55-57</sup> M-Sb (M= Al, Cu, Zn, Mo and Bi),<sup>58-62</sup> and M-P (M= Fe, Ni)<sup>63,64</sup> alloys have been explored as anode for NIBs. For instance, Yu and Maier<sup>56</sup> successfully prepared highly porous Ni<sub>3</sub>Sn<sub>2</sub> microcages composed of tiny nanoparticles through a facile template-free solvothermal method. As anode for NIBs, it maintained a reversible capacity of 270 mA h g<sup>-1</sup> at the rate of 1 C for 300 cycles. The outstanding performance is attributed to shortened ion-diffusion distance, good electronic conductivity and suppressed mechanical strain of Sn by the hollow cores structure and Ni matrix.

The fourth key approach is to fabricate M-(Sn, Sb, P, Ge) alloys, in which M is an electrochemically active component. In this system, the two different metal phases can work as mutual buffer to each other to alleviate the volume fluctuation. SnSb<sup>65-67</sup> and Sn<sub>4</sub>P<sub>3</sub><sup>68-70</sup> have been extensively applied to NIBs.

SnSb was first developed as anode for NIBs by Liu's group.<sup>65</sup> It was found that the alloying/dealloying reactions occurred in a sequential manner. That is, SnSb was first sodiated to form amorphous Na<sub>3</sub>Sb<sup>66</sup> and Sn, followed by the sodiation of Sn into Na<sub>15</sub>Sn<sub>4</sub>. The coexisting Sn- and Sb-rich phases generated during sequential reactions can self-support one another. As a result, the SnSb electrode can maintain the stability and good electric contact during the sodiation/desodiation processes. Therefore, the high initial capacity (544 mA h g<sup>-1</sup>) and good cyclability (80% capacity retention over 50 cycles at of 100 mA g<sup>-1</sup>) can be reached. Additionally, Sn-Ge-Sb ternary alloy was also prepared for NIBs with high capacity, excellent cyclability and rate capability.<sup>71</sup>

Sn<sub>4</sub>P<sub>3</sub> was firstly reported as anode for NIBs by Lee's group.<sup>68</sup> Sn<sub>4</sub>P<sub>3</sub> exhibited a high reversible capacity of 718 mA h g<sup>-1</sup> with negligible capacity fading over 100 cycles. It was shown that Sn<sub>4</sub>P<sub>3</sub> was firstly converted into Na<sub>x</sub>P and NaSn during sodiation, and NaSn further sodiated to form Na<sub>15</sub>Sn<sub>4</sub> after full sodiation. The excellent electrochemical performance of Sn<sub>4</sub>P<sub>3</sub> was attributed to synergistic sodium storage reactions of the Sn and P components, where Sn-based phase worked as electronic channels to enhance electrical conductivity of the P component, while the elemental P and Na<sub>x</sub>P acted as a shielding matrix to relieve the volume expansion during Na insertion reaction.

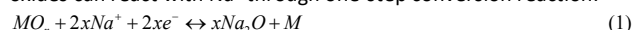
The fifth significant approach is to use proper electrolyte additive, such as fluoroethylene carbonate (FEC).<sup>38, 40, 41, 72, 73</sup> Liu's group deeply studied the formation of solid electrolyte interphase (SEI) layers of SnSb system. It was revealed that the presence of FEC can largely minimize the electrolyte decomposition, modify the morphology, structure and chemical composition of the surface passivation layer and finally result in the formation of thin, uniform, stable and structurally compact SEI films. These films contributed to stabilizing electrode and improving migration kinetics of Na<sup>+</sup> ions, leading to remarkable cycle stability and excellent rate performance.<sup>73</sup> Darwiche<sup>38</sup> *et al* studied the electrochemistry performance of bulk Sb with and without FEC. Sb delivered a high capacity of 576 mA h g<sup>-1</sup> over 160 cycles at 0.5 C and an extremely good coulombic efficiency exceeding 98% with electrolyte additive of FEC, while the capacity decayed steeply after 15 cycles when this

additive was not added (Fig. 4c). In addition, the novel electrolyte with two additives of fluoroethylene carbonate (FEC) and tris(trimethylsilyl)phosphate (TMSP) can achieve observably improvement in the electrochemical performance of Sn<sub>4</sub>P<sub>3</sub> anode for NIBs.<sup>74</sup>

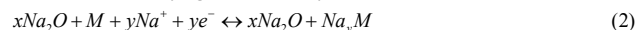
Finally, using three-dimensionally cross linkable binders, such as polyacrylic acid (PAA)<sup>72</sup> and carbxyethyl cellulose (CMC)<sup>45</sup> is also an effective way to promote the cycling performance. Komaba *et al.* demonstrated the capacity and coulombic efficiency of Sn electrode were improved by utilizing the PAA binder instead of PVDF.<sup>72</sup>

#### 4 Metal oxides and sulfides

Recently, more and more metal oxides (denoted as MO<sub>x</sub>) have been studied as anodes for NIBs. In this section, we focus on those metal oxides storing Na via conversion reactions. The reaction mechanism can be summed up into two types according to the electrochemically inactive or active metal in an oxide. If the metal is an inactive element, such as, Fe, Co, Ni, Cu, Mn, and Mo, metal oxides can react with Na<sup>+</sup> through one-step conversion reaction:



When the metal is electrochemically active, such as Sn, and Sb, metal oxides can react with Na<sup>+</sup> via a conversion reaction (eqn (1)) and a further alloying reaction (eqn (2)).



These anodes show high capacities and energy densities due to the multi-electron reactions. However, they also troubled with low initial coulombic efficiency, large hysteresis and poor cyclability. Recently, various nanostructured MO<sub>x</sub><sup>75-77</sup> and MO<sub>x</sub>/C composites<sup>78-81</sup> (as summarized in Table 3) have been synthesized to solve these issues.

In 2002, transition metal oxide spinel NiCo<sub>2</sub>O<sub>4</sub> was first reported as anode for NIBs. *Ex-situ* XRD analysis demonstrated that NiCo<sub>2</sub>O<sub>4</sub> transformed to metal Co and Ni after full sodiation. NiCo<sub>2</sub>O<sub>4</sub> delivered a reversible capacity of ca. 200 mA h g<sup>-1</sup>, which was much lower than the theoretical capacity (890 mA h g<sup>-1</sup>). In addition, reversible discharge capacity of about 300 mA h g<sup>-1</sup> was obtained in a full sodium cell using spinel NiCo<sub>2</sub>O<sub>4</sub> versus layered Na<sub>x</sub>CoO<sub>2</sub>.<sup>82</sup>

Fe<sub>2</sub>O<sub>3</sub> and Fe<sub>3</sub>O<sub>4</sub> are attractive anodes due to their high theoretical capacity and low cost. Komaba *et al.* firstly testified that the nanocrystallized Fe<sub>3</sub>O<sub>4</sub> and α-Fe<sub>2</sub>O<sub>3</sub> were electrochemically active in the sodium salt electrolyte, however, the obtained sodium storage capacity was rather low.<sup>83</sup> Fe<sub>2</sub>O<sub>3</sub> nanocrystals anchored onto graphene nanosheets (Fe<sub>2</sub>O<sub>3</sub>@GNS) were prepared by a nanocasting technique. As anode for NIBs, Fe<sub>2</sub>O<sub>3</sub>@GNS exhibited an initial capacity of 535 mA h g<sup>-1</sup> and 75% capacity retention after 200 cycles at 100 mA g<sup>-1</sup>. However, the initial coulombic efficiency was low.<sup>78</sup> On a different approach, Chen's group prepared porous γ-Fe<sub>2</sub>O<sub>3</sub>@C nanocomposite by a simple aerosol spray pyrolysis, where ultra small γ-Fe<sub>2</sub>O<sub>3</sub> nanoparticles (~5 nm) were uniformly dispersed in a porous carbon matrix. The obtained product exhibited high sodium storage capacity (740 mA h g<sup>-1</sup> at 200 mA g<sup>-1</sup>), outstanding cyclability (358 mA h g<sup>-1</sup> after 1400 long cycles at 2000 mA h g<sup>-1</sup>) and high-rate capability (317 mA h g<sup>-1</sup> at high rate of 8000 mA g<sup>-1</sup>).<sup>79</sup> Recently, a full Na-ion cell based on a Fe<sub>3</sub>O<sub>4</sub>/C anode, Na[Ni<sub>0.25</sub>Fe<sub>0.5</sub>Mn<sub>0.25</sub>]O<sub>2</sub> cathode and novel electrolyte (NaClO<sub>4</sub> in ethyl methanesulfonate (EMS)/fluoroethylene carbonate (FEC)) was

examined, delivering a capacity of 130 mA h g<sup>-1</sup> and 76.1 % capacity retention after 150 cycles (Fig. 5a).<sup>84</sup>

More strikingly, CuO as anode for NIBs have made great progress. Chen's group prepared porous CuO nanowires composed of nanoparticles (~50 nm), which showed a capacity of 303 mA h g<sup>-1</sup> for 50 cycles at a current density of 50 mA h g<sup>-1</sup>.<sup>75</sup> As shown in Fig. 5b, during the initial sodiation process, two irreversible peaks (1.08 and 0.36) were ascribed to the decomposition of electrolyte and the formation of a SEI layer. In the subsequent cycles, the cathodic peaks at 1.64, 0.60 and 0.16 V corresponded to three electrochemistry reactions: Na<sup>+</sup> ions firstly reacted with CuO to form Cu<sup>I</sup><sub>1-x</sub>Cu<sup>II</sup><sub>x</sub>O<sub>1-x/2</sub> and Na<sub>2</sub>O, Na<sup>+</sup> further inserted into Cu<sup>II</sup><sub>1-x</sub>Cu<sup>I</sup><sub>x</sub>O<sub>1-x/2</sub> to produce Cu<sub>2</sub>O, and finally to form Cu nanoparticles embedded in Na<sub>2</sub>O matrix after full sodiation. In order to improve the cycling stability of CuO, their group further designed the CuO/C spheres. They delivered a significantly improved electrochemical properties, with a high capacity of 402 mA h g<sup>-1</sup> after 600 cycles at 200 mA g<sup>-1</sup> and 304 mA h g<sup>-1</sup> at a high rate of 2000 mA g<sup>-1</sup>.<sup>80</sup> In addition, porous CuO nanorod arrays (CNAs) were fabricated by *in situ* engraving commercial copper foils, which could be directly employed as anode without binder and conductive agent for NIBs.<sup>76</sup>

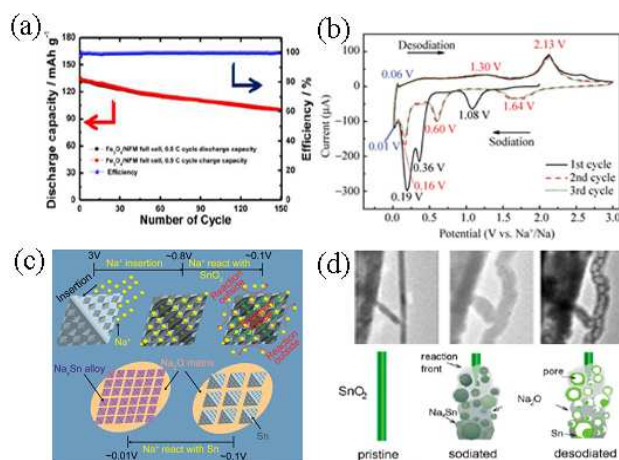


**Fig. 5** (a) Cycle performance for the Fe<sub>3</sub>O<sub>4</sub>/Na[Ni<sub>0.25</sub>Fe<sub>0.5</sub>Mn<sub>0.25</sub>]O<sub>2</sub> full cell. (b) Cyclic voltammograms of CuO nanowires from 0.01 to 3.0 V at a scan rate of 0.1 mV s<sup>-1</sup>. (c) The schematic illustration of the mechanism for the initial discharge process of SnO<sub>2</sub> nanocrystals in a Na-ion cell. (d) TEM images and schematic drawing show the structural evolution of the nanowire during sodiation/desodiation. (a) reprinted with permission from ref. 84. Copyright 2014 American Chemical Society. (b) reprinted with permission from ref. 75. Copyright 2014 Tsinghua University Press and Springer-Verlag Berlin Heidelberg. (c) reproduced from ref. 97 with permission from the PCCP Owner Societies. (d) reprinted with permission from ref. 101. Copyright 2013 American Chemical Society.

Moreover, many groups devote their effort to exploring the Na storage performance of Co<sub>3</sub>O<sub>4</sub>.<sup>77, 85, 86</sup> For example, nanostructured Co<sub>3</sub>O<sub>4</sub> showed a reversible capacity of 447 mA h g<sup>-1</sup> for 50 cycles at 25 mA g<sup>-1</sup> between 0.01-3.0 V.<sup>83</sup> Similar to the lithiation of Co<sub>3</sub>O<sub>4</sub>, a characteristic discharge plateau at a lower voltage of 0.01 V (vs. Na<sup>+</sup>/Na) was found, however, the sodiation plateau was not as marked as that caused by lithiation. Additionally, many other metal oxides based on conversion reaction have also been investigated,

such as NiO,<sup>87, 88</sup> MoO<sub>3</sub>,<sup>89, 90</sup> and Mn<sub>2</sub>O<sub>3</sub>.<sup>91</sup> Above all, a positive effect of the PAA/CMC binder to improve the electrochemical performance of oxide-based anodes in Na cell was demonstrated.<sup>92</sup>

Most of the above metal oxides with electrochemically inactive metal element show the reversible capacities no high than 500 mA h g<sup>-1</sup>. When it comes to metal oxides consisting of active metal element, the capacity will be much higher due to further alloying reaction.

Sn based metal oxides (SnO and SnO<sub>2</sub>) have proved to be promising anode for NIBs.<sup>93-99</sup> Shimizu *et al.* first reported the Na storage performance of SnO thick film, which exhibited an initial capacity of 580 mA h g<sup>-1</sup>, but only 260 mA h g<sup>-1</sup> after 50 cycles at 50 mA g<sup>-1</sup>.<sup>100</sup> Subsequently, hierarchical mesoporous SnO microspheres with better electrochemical performance were also prepared by Wang's group.<sup>93</sup> SnO microspheres were composed of mesoporous nanosheets (~20 nm in thickness) and each nanosheet consisting of SnO nanocrystals (~10 nm) which were exposed with {001} facets. This unique structure would facilitate Na<sup>+</sup> diffusion. As a result, a high capacity of 371 mA h g<sup>-1</sup> after 50 cycles at 40 mA g<sup>-1</sup> was obtained. *Ex situ* XRD revealed that Na<sup>+</sup> first inserted into SnO to form crystalline tetragonal Sn, then the Sn further alloyed with Na<sup>+</sup> to produce NaSn<sub>2</sub>. Moreover, their team also made a great deal of research on SnO<sub>2</sub>. For example, SnO<sub>2</sub>@graphene composite was prepared by *in situ* hydrothermal method and gave a high Na storage capacity of more than 700 mA h g<sup>-1</sup> for 100 cycles at 20 mA g<sup>-1</sup>.<sup>95</sup> Furthermore, they studied the Na storage mechanism of SnO<sub>2</sub> by *ex situ* TEM and it was found that Na ion inserted into the SnO<sub>2</sub> to generate NaSnO<sub>2</sub> (above 0.8 V). After that, Na<sup>+</sup> further inserted into NaSnO<sub>2</sub> to form Na<sub>2</sub>O and Sn (0.8-0.1 V) and finally Sn alloyed with Na to form Na<sub>x</sub>Sn (0.1-0.01 V) (As illustrated in Fig. 5c).<sup>97</sup>

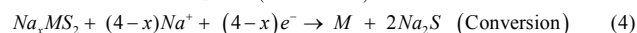
More importantly, *in situ* TEM has been utilized to probe the failure mechanism of SnO<sub>2</sub> nanowire.<sup>101</sup> As shown in Fig. 5d, upon sodiation, Na inserted into SnO<sub>2</sub> to form the structure, where Na<sub>x</sub>Sn particles were embedded in the Na<sub>2</sub>O matrix, accompanying with huge volume expansion. Upon desodiation, the Na<sub>x</sub>Sn transformed into Sn nanoparticles surrounded by pores. These pores largely increased electrical impedance, leading to the poor cycling stability of SnO<sub>2</sub>. And fast sodiation was also observed in the misoriented surface grains owing to the promoted Na<sup>+</sup> transport along the grain boundaries.

More recently, various of Sb based metal oxides have been examined as anode for NIBs, such as Sb<sub>2</sub>O<sub>3</sub>,<sup>102</sup> SbO<sub>x</sub>,<sup>103</sup> and Sb<sub>2</sub>O<sub>4</sub>.<sup>104</sup> Compared to tin oxides, antimony oxides exhibit more satisfied cyclability. For example, Hu *et al.* first reported Sb<sub>2</sub>O<sub>3</sub> anode for NIBs, which performed remarkable cycling stability with a capacity of 414 mA h g<sup>-1</sup> at 500 mA g<sup>-1</sup> after 200 cycles between 0.01-2 V. Based on the results of XRD, HR-TEM, SAED and XPS, it was found Na<sup>+</sup> initially intercalated into Sb<sub>2</sub>O<sub>3</sub> without structural change, (above 0.8 V) and then Sb<sub>2</sub>O<sub>3</sub> further reacted with Na<sup>+</sup> to form Sb and Na<sub>2</sub>O (0.8-0.4 V). Finally, NaSb was produced after full sodiation. Li *et al.* further improved the performance of Sb<sub>2</sub>O<sub>3</sub> by fabricating Sb<sub>2</sub>O<sub>3</sub>/Sb@graphene nanocomposites anchored on 3D carbon sheet network, which exhibited 92.7% desodiation capacity retention after 275 cycles.<sup>102</sup>

Metal sulfides (MS<sub>n</sub>) are also widely studied anode materials. In general, the mechanism in Na-MS<sub>n</sub> occurs through two steps. Na<sup>+</sup> first intercalates into MS<sub>n</sub> to form an intermediate (Na<sub>x</sub>MS<sub>n</sub>), then

$\text{Na}_x\text{MS}_2$  decomposes to  $\text{Na}_2\text{S}$  and  $\text{M}$  through a conversion reaction.<sup>105-107</sup> However, the latter conversion reaction usually causes severe volume expansion of the electrode materials and sluggish kinetics for  $\text{Na}^+$  intercalation/de-intercalation.<sup>107, 108</sup> Many approaches, such as preparing  $\text{MS}_2/\text{C}$  composites, controlling the cut-off voltage, have been adopted to solve these problems. Generally speaking, Metal sulfides are composed of layered metal disulfides and non-layered metal sulfides.

Layered metal disulfides ( $\text{M} = \text{Mo}, \text{Sn}, \text{W}, \text{Ti}$ ) in which a layer of metal atoms ( $\text{M}$ ) sandwiched between two layers of  $\text{S}$ . Strong covalent bonding characterizes the  $\text{M-S}$  interactions, while the interactions between  $\text{S-M-S}$  single-layers are characterized by weak Van der Waals forces. Therefore, layered  $\text{MS}_2$  is expected as a promising intercalation host material for NIBs. In a  $\text{Na-MS}_2$  system, the reaction conducts as the following:



$\text{MoS}_2$ , a typical layered material, has been intensively investigated as anode for NIBs. Park *et al.* firstly explored the Na storage property of bulk  $\text{MoS}_2$ , however, only  $89 \text{ mA h g}^{-1}$  after 100 cycles was obtained.<sup>109</sup> One approach to improve the specific capacity is preparing few-layered or even single-layered  $\text{MoS}_2$ , which can relieve the strain and decrease the barrier for  $\text{Na}^+$  intercalation.<sup>106, 110</sup> The other one is fabricating  $\text{MoS}_2/\text{carbon}$  composites to promote electrochemical kinetics and alleviate volume variations.<sup>106, 110, 111-114</sup> For example,  $\text{MoS}_2/\text{graphene}$  composite paper, in which few-layered  $\text{MoS}_2$  nanoflakes were dispersed in graphene matrix, was directly utilized as anode for NIBs, which exhibited a capacity of  $230 \text{ mA h g}^{-1}$  after 20 cycles at  $250 \text{ mA g}^{-1}$ .<sup>110</sup> Wang's group demonstrated that  $\text{MoS}_2/\text{graphene}$  heterointerface played a key role in improving the conductivity of  $\text{MoS}_2$ , increasing Na-storage capacity.<sup>115</sup> This work deepened the understanding of 2D graphene-based heterostructure and lay the foundation for rational design high performance materials for NIBs. Maier's group further improved the reversible capacity by synthesizing single-layered ultrasmall  $\text{MoS}_2$  nanoplates embedded in carbon nanowires (Fig. 6a-d). The obtained electrode exhibited an ultrahigh capacity of  $854 \text{ mA h g}^{-1}$  at  $100 \text{ mA g}^{-1}$  and  $253 \text{ mA h g}^{-1}$  at a high rate of  $10 \text{ A g}^{-1}$  for 100 cycles (Fig. 6e). This excellent Na-storage capability could be attributed to the ultrasmall reaction domains, which allowed for a nearly diffusionless and nucleation-free "conversion".<sup>106</sup> Moreover, the cycling stability of  $\text{MoS}_2$  was largely improved by controlling the cut-off voltage to the range of 0.4-3 V, during which only reversible intercalation reaction (eqn (3)) took place.<sup>107</sup>

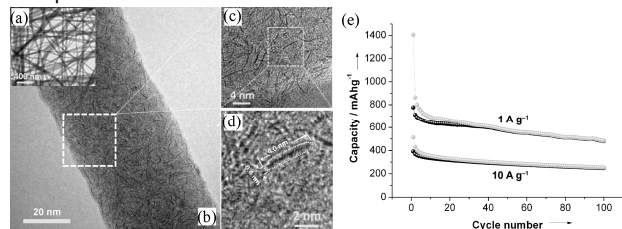


**Fig. 6** (a-d) TEM, HTEM images and (e) excellent cycling performance of single layered  $\text{MoS}_2$ -carbon nanofiber composite. Reprinted with permission from ref. 106. Copyright 2014 Wiley-VCH Verlag GmbH & Co. KGaA, Weinheim.

More impressively, the structure evolutions of  $\text{MoS}_2$  during the intercalation were clarified at the atomic scale by advanced aberration-corrected scanning transmission electron microscopy (STEM).<sup>105</sup> Just as shown in Fig 7, upon discharge,  $\text{Na}^+$  first intercalated to every other interlayer of few-layered 2H- $\text{MoS}_2$  (Fig. 7b, 7f and 7j), then intercalated into the empty layers (Fig. 7c, 7g and 7k) before the former interlayers were fully occupied. Meanwhile, the sulfur planes glide along an interlayer atomic plane to produce 1T- $\text{MoS}_2$ . And finally  $\text{Na}^+$  filled all the interlayers (Fig. 7d, 7h and 7l) of  $\text{MoS}_2$  (Fig. 7a, 7e and 7i). It was also shown that when more than 1.5  $\text{Na}^+$  per formula of  $\text{MoS}_2$  were intercalated,  $\text{Na}_x\text{MoS}_2$  would decompose to  $\text{Na}_2\text{S}$  and  $\text{Mo}$ , and the structural evolution would be irreversible. Furthermore, a planar microscale battery was designed to study the topographical changes of  $\text{MoS}_2$  during cycle process.<sup>116</sup> Atomic force microscopy (AFM) revealed that the permanent structural wrinkling of sodiated  $\text{MoS}_2$  was observed at 0.4 V, while SEI layer on the  $\text{MoS}_2$  electrode formed around 1.5 V with an average thickness of  $20.4 \text{ nm} \pm 10.9 \text{ nm}$  before sodium intercalation.

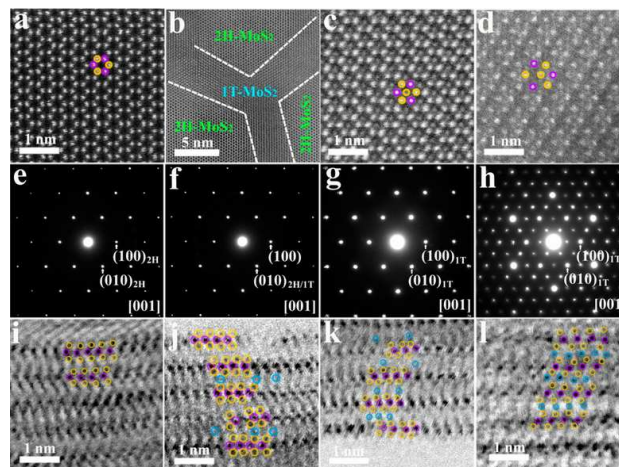
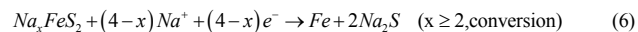
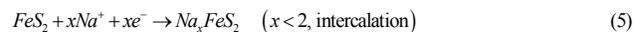


**Fig. 7** High-angle annular dark-field (HAADF), and selected area electron diffraction (SAED) images of commercial  $\text{MoS}_2$  in Cell-60 (a and e), Cell-80 (b and f), Cell-160 (c and g), and Cell-256 (d and h) along the [001] zone axis and the annular brightfield (ABF) images of as-prepared nano- $\text{MoS}_2$  (i) with cutoff at 1.0 V (j), 0.8 V (k), and 0.2 V (l) along the [100] zone axis. The purple, yellow, and blue circles are overlaid in the image for Mo, S, and Na atoms, respectively. Reprinted with permission from ref. 105. Copyright 2014 American Chemical Society.

Recently, non-layered metal sulfides, such as  $\text{FeS}_2$ ,<sup>125, 126</sup>  $\text{Sb}_2\text{S}_3$ ,<sup>127</sup>  $\text{Ni}_3\text{S}_2$ ,<sup>128</sup> have also exhibited promising electrochemistry properties for NIBs. For a  $\text{Na-FeS}_2$  cell, the reaction also proceeds in two steps:



For a long time,  $\text{FeS}_2$  had characterized with bad cyclability due to the huge volume change (mainly generated by conversion reaction) and improper electrolyte.<sup>129</sup> Very recently, Hu *et al.* discovered that the detrimental conversion reaction (eqn (6)) in a  $\text{Na/FeS}_2$  battery could be avoided through controlling the cut-off voltage to 0.8 V and using  $\text{NaSO}_3\text{CF}_3/\text{diglyme}$  electrolyte. As a result, an unprecedented long-term cycling stability ( $\sim 90\%$  capacity retention at  $1 \text{ A g}^{-1}$  for 20000 cycles) and remarkable high-rate capability

( $\sim 170 \text{ mA h g}^{-1}$  at  $20 \text{ A g}^{-1}$ ) were achieved.<sup>108</sup>  $\text{Sb}_2\text{S}_3$  exhibited a high capacity of  $835.3 \text{ mA h g}^{-1}$  at  $50 \text{ mA g}^{-1}$  over 50 cycles and  $553.1 \text{ mA h g}^{-1}$  at a high rate of  $2000 \text{ mA g}^{-1}$ .<sup>127</sup> However, the electrochemistry performance of  $\text{Ni}_3\text{S}_2$  in Na-cell was far from satisfying.<sup>128</sup>

## 5 Titanium-based compounds

Recently, various titanium-based compounds have been explored as promising sodium insertion host due to their low-cost, nontoxicity, low operation voltage, low strain and excellent cyclability. However, the performances of them strongly depend on the electrolyte,<sup>130</sup> the binder<sup>92,131-133</sup> and the morphology.<sup>134</sup> In general, Ti-based composites provides low specific capacity due to the limited Na storage sites. The main achievements for titanium-based composites, such as  $\text{TiO}_2$ ,  $\text{Na}_2\text{Ti}_3\text{O}_7$ ,  $\text{Na}_4\text{Ti}_5\text{O}_{12}$ ,  $\text{Li}_4\text{Ti}_5\text{O}_{12}$ , and  $\text{Na}_2\text{Ti}_6\text{O}_{13}$ , are reviewed in this section.

Titanium dioxide ( $\text{TiO}_2$ ) has several main polymorphs such as anatase, rutile, brookite and  $\text{TiO}_2(\text{B})$ . Among them, anatase  $\text{TiO}_2$  is most widely investigated for NIBs because of its three dimensional open structure. Xu *et al.* firstly reported that nanocrystalline anatase  $\text{TiO}_2$  composite was able to store Na and delivered a high reversible capacity of  $150 \text{ mA h g}^{-1}$  for 100 cycles (Fig. 8a).<sup>135</sup> Subsequently, various mechanisms of anatase  $\text{TiO}_2$  in Na cells have been reported. Kim<sup>134</sup> and Cha<sup>136</sup> *et al.* demonstrated that  $\text{Na}^+$  reacted with  $\text{TiO}_2$  based on an intercalation reaction accompanying with a reversible  $\text{Ti}^{4+/3+}$  redox reaction. On the contrary, Passerini's group<sup>137</sup> reported that: anatase  $\text{TiO}_2$  irreversibly converted into metallic titanium (detected by XPS), sodium superoxide (by SEM-EDX) and an amorphous sodium titanate phase; successively,  $\text{Na}^+$  ions were able to reversibly de/intercalate from/into the newly formed sodium titanate phase, which was responsible for the capacity of the following cycles. Bronze-type  $\text{TiO}_2$  nanotube was firstly explored as anode in Na batteries by Gao's group.<sup>138</sup> They found only the large interlayer spacing of (001) plane in  $\text{TiO}_2(\text{B})$  could accommodate sodium ions while lithium ion could be stored in interlayer spacing of both (001) and (110) planes. Thus,  $\text{TiO}_2(\text{B})$  showed a low capacity of only  $50 \text{ mA h g}^{-1}$  after 90 cycles. In addition, hollandite-type  $\text{TiO}_2$  electrode showed a low capacity of  $85 \text{ mA h g}^{-1}$  (corresponding to the insertion of 0.25 Na per formula) for 11 cycles in the voltage range of 2.5-0.2 V.<sup>139</sup> XRD and in situ SXRD demonstrated that  $\text{Na}^+$  initially inserted into  $\text{TiO}_2(\text{H})$  via a single-phase process, then the structural phase of  $\text{TiO}_2(\text{H})$  changed from tetragonal symmetry to monoclinic symmetry with more  $\text{Na}^+$  insertion. More importantly, many approaches has been attempted to promote the properties of  $\text{TiO}_2$ , such as choosing proper binder<sup>92</sup> and electrolyte,<sup>133</sup> heteroatom doping (Fig. 8b)<sup>140-142</sup> designing low-dimension  $\text{TiO}_2$ <sup>142, 143</sup> and carbon coated composites.<sup>136, 144</sup>

Spinel  $\text{Li}_4\text{Ti}_5\text{O}_{12}$ , the "zero-strain" anode for LIBs, was first introduced and further studied as anode for NIBs by Zhao and Sun<sup>131, 145</sup> As shown in Fig. 8c,  $\text{Li}_4\text{Ti}_5\text{O}_{12}$  with CMC binder showed highest reversible capacity of  $155 \text{ mA h g}^{-1}$  with a long discharge plateau at  $\sim 0.7 \text{ V}$ . The electrodes with sodium alginate (NaAlg) binder exhibited a lower capacity. However, the capacity declined steeply for conventional PVdF electrodes. Theory DFT calculations and experiment investigations demonstrated that  $\text{Na}^+$  inserted into  $\text{Li}_4\text{Ti}_5\text{O}_{12}$  via a three-phase separation mechanism (Fig. 8d, as given

in eqn(9)). In addition, the sodium storage behavior of  $\text{Li}_4\text{Ti}_5\text{O}_{12}$  strongly depend on composite nanosize,<sup>146</sup> testing temperature<sup>147</sup> and pseudocapacitance effect.<sup>148</sup> Inspired by these promising results, sodium based analogues with the same stoichiometry ( $\text{Na}_4\text{Ti}_5\text{O}_{12}$ ) have also been investigated. Nevertheless, it provided a rather low capacity of  $56 \text{ mA h g}^{-1}$  for 50 cycles.<sup>149</sup>

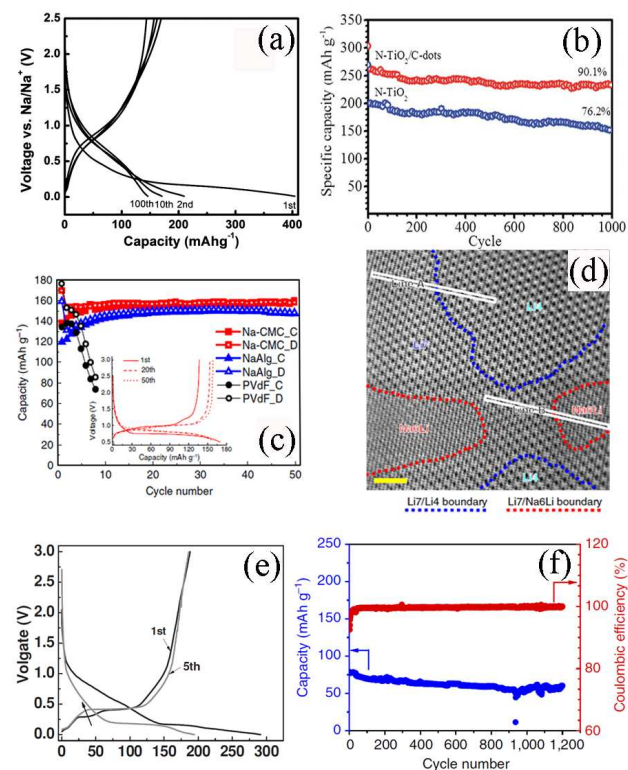
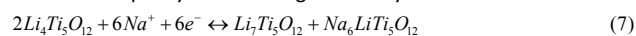


**Fig. 8** (a) Charge–discharge profiles of Anatase  $\text{TiO}_2$  Nanocrystals, at  $50 \text{ mA g}^{-1}$  (b) Cycling performance of N-doped  $\text{TiO}_2$  nanorods decorated with carbon dots at 2 C. (c) Cyclic performances of  $\text{Li}_4\text{Ti}_5\text{O}_{12}$  electrode with different binders (inset discharge/charge profiles of Na-CMC electrode). (d) ABF image in the half electrochemically sodiated  $\text{Li}_4\text{Ti}_5\text{O}_{12}$  nano-particle. (e) The charge/discharge curves of the  $\text{Na}_2\text{Ti}_3\text{O}_7$  electrode. (f) Long-term cycling performance of  $\text{P2-Na}_{0.66}[\text{Li}_{0.22}\text{Ti}_{0.78}]\text{O}_2$  electrodes. (a) reproduced from ref. 135 with permission from The Royal Society of Chemistry. (b) reproduced from ref. 140 with permission from The Royal Society of Chemistry. (c, d) reprinted with permission from Macmillan Publishers Ltd.: (*Nat. Commun.*) (ref. 131), copyright 2013. (e) reprinted with permission from ref. 151. Copyright 2013 Wiley-VCH Verlag GmbH & Co. KGaA, Weinheim. (f) reprinted with permission from Macmillan Publishers Ltd.: (*Nat. Commun.*) (ref. 157), copyright 2013.

Layered sodium titanium oxide,  $\text{Na}_2\text{Ti}_3\text{O}_7$ , was first examined as anode for NIBs by Senguttuvan.<sup>150</sup> As shown in Fig. 8e, upon discharge,  $\text{Na}_2\text{Ti}_3\text{O}_7$  transforms to  $\text{Na}_4\text{Ti}_3\text{O}_7$  (about  $200 \text{ mA h g}^{-1}$ ) at a low plateau around  $0.3 \text{ V}$  (vs.  $\text{Na}^+/\text{Na}$ ), which is the lowest intercalation potential among reported oxides. By optimizing the composition of electrolyte and binder, microsized  $\text{Na}_2\text{Ti}_3\text{O}_7$  offered

a high initial capacity of  $188 \text{ mA h g}^{-1}$  at  $20 \text{ mA g}^{-1}$  in  $1 \text{ M NaFSI/PC}$  electrolyte with  $\text{NaAlG}$  binder, but the cycling stability is poor.<sup>151</sup> Additionally, DFT calculations demonstrated that the activation energy of  $\text{Na}^+$  diffusion between  $\text{TiO}_6$  octahedron layers was fairly low ( $0.186 \text{ eV}$ ). A spider web-like  $\text{Na}_2\text{Ti}_3\text{O}_7$  nanotube was directly utilized as anode without binder, delivering improved cyclability but low initial coulombic efficiency.<sup>152</sup> Notably, cyclability and coulombic efficiency can be remarkably enhanced by carbon coating.<sup>153,154</sup>

$\text{Na}_2\text{Ti}_6\text{O}_{13}$ , with a two dimensional layered structure, has also been studied as a promising sodium intercalation host. It stored  $\text{Na}^+$  following a solid-solution mechanism.<sup>155, 156</sup> Rudola *et al.* prepared  $\text{Na}_2\text{Ti}_6\text{O}_{13}$  nanorods by a soft-template method.<sup>155</sup> When used as anode for NIBs, it showed a reversible capacity of more than  $40 \text{ mA h g}^{-1}$  (corresponding to  $0.85 \text{ Na}^+$  ions insertion per formula unit) with a plateau at around  $0.8 \text{ V}$  in the voltage range of  $0.5\text{--}2.5 \text{ V}$ .  $\text{Na}_2\text{Ti}_6\text{O}_{13}$  electrodes with graphite conductive additive revealed a surprising cycling stability with  $85 \%$  capacity retention for  $5000$  cycles at  $20 \text{ C}$ , but the capacity is quite low. By lowering the cut-off voltage to  $0 \text{ V}$ , a high initial capacity of  $200 \text{ mA h g}^{-1}$  was obtained but faded rapidly.<sup>156</sup>

More impressively, P2-type layered  $\text{Na}_{0.66}[\text{Li}_{0.22}\text{Ti}_{0.78}]\text{O}_2$  was synthesized and explored in NIBs.<sup>157</sup> It delivered a reversible capacity of  $116 \text{ mA h g}^{-1}$  (corresponding to  $0.38 \text{ Na}^+$  ions insertion per formula unit) at an average storage potential of  $0.75 \text{ V}$ . It is worth noting that the volume change during  $\text{Na}^+$  insertion/extraction is only  $0.77 \%$ , nearly zero-strain. As a result, an ultra long cycle life with  $75 \%$  capacity retention after  $1200$  cycles was achieved (Fig. 8f). Additionally,  $\text{Na}_{0.66}[\text{Li}_{0.22}\text{Ti}_{0.78}]\text{O}_2$  proceeded through a quasi-single-phase electrochemical mechanism, which is different from other P2-type materials. Also, many other titanium-based composites, such as  $\text{NaTi}_3\text{O}_6\text{OH}\cdot 2\text{H}_2\text{O}$ ,<sup>158, 159</sup>  $\text{MgTi}_2\text{O}_5$ ,<sup>160</sup> have also been investigated in Na cell with good electrochemistry properties.

## 6 Organic composites

Organic electrode materials have attracted growing attentions due to the following merits: the abundant resources from biomass, tremendous chemical compounds, structural flexibility and possible multi-electron reactions.<sup>1, 161</sup> However, they also associated with high solubility and sluggish kinetics. The previously reported organic composites with effective Na activity include disodium terephthalate ( $\text{Na}_2\text{C}_8\text{H}_4\text{O}_4$ ),<sup>162, 163</sup> disodium 2,5-dihydroxy-1,4-benzoquinone ( $\text{Na}_2\text{C}_6\text{H}_2\text{O}_4$ ),<sup>164</sup> disodium naphthalenediimide ( $\text{Na}_2\text{C}_{14}\text{H}_4\text{O}_4\text{N}_2$ ),<sup>165</sup> sodium 4,4'-stilbene-dicarboxylate ( $\text{Na}_2\text{C}_{16}\text{H}_{10}\text{O}_4$ ),<sup>166</sup> 4,4-Biphenyldicarboxylate sodium ( $\text{Na}_2\text{C}_{14}\text{H}_8\text{O}_4$ ),<sup>167</sup> tetrasodium salt of 2,5-dihydroxyterephthalic acid ( $\text{Na}_4\text{C}_8\text{H}_4\text{O}_4$ )<sup>168</sup> and polymeric schiff bases ( $-\text{N}=\text{CH}-\text{Ar}-\text{HC}=\text{N}-$ )<sup>169</sup>. For example, Wang *et al.*<sup>166</sup> successfully designed an extended  $\pi$ -conjugated system (sodium 4,4'-stilbene-dicarboxylate, Fig. 9a) to solve the current challenge of fast-charge/-discharge. As shown in Fig. 9b, the molecules stacked layer-by-layer with  $\pi$ - $\pi$  intermolecular interaction and carboxylate group located on the surface of the layers, building a channel for  $\text{Na}^+$  insertion/extraction. It delivered a discharge plateau at  $0.45 \text{ V}$  due to redox of the two carbonyl groups (Fig. 9c) and high reversible capacity of  $220 \text{ mA h g}^{-1}$  at  $50 \text{ mA g}^{-1}$ .

Outstanding rate capability and remarkable long cycle life were also demonstrated. A capacity of  $72 \text{ mA h g}^{-1}$  at an ultra high rate of  $10 \text{ A g}^{-1}$  and more than  $70 \%$  capacity retention at  $1 \text{ A g}^{-1}$  for  $400$  cycles were obtained.

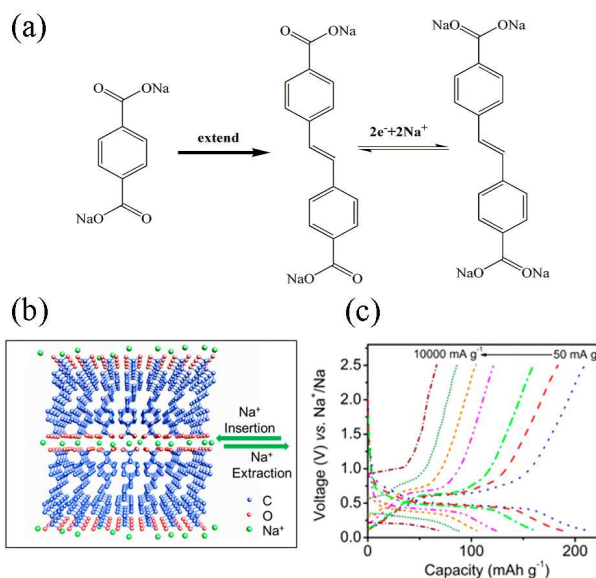


**Fig. 9** (a) Schematic chemical structure of starting molecule SBDC, extended product SSDC and reaction mechanism of SSDC. (b) Schematic molecular packing of SSDC (c) rate capability of SSDC. Reprinted with permission from ref. 166. Copyright 2015 American Chemical Society.

## 7 Conclusions and perspectives

With the increasing demand for energy and steep consumption of lithium resources, Na-ion batteries have caught peoples' attention once again, owing to their low cost and the natural abundance of sodium resources. NIBs are promising to be applied to large-scale energy storage system, where weight is not critical. However, challenges still remain, especially for anode, before NIBs are commercial. The electrochemistry performances of several layered-oxides as cathode for NIBs have been able to compete with those of their lithium analogues, however, the graphite, which was widely used in commercial LIBs, fails to intercalate  $\text{Na}^+$  ions efficiently. Encouragingly, expanded graphite with interlayer distance of  $4.3 \text{ \AA}$  exhibits improved Na-storage performance. This provides us a new method to tailor graphite for NIBs. Disorder carbon with large interlayer distance also shows highly Na activity. Nevertheless, the specific capacity of carbonaceous materials is generally low, no more than  $300 \text{ mA h g}^{-1}$ . Also, the sodiation voltage ( $\sim 0 \text{ V}$ ) for hard carbon is too low, resulting in major safety concerns during fast charging process. Considering the cost, research achievements and relative mature technology in commercial LIBs, carbonaceous materials are still key focus area in future. Alloy-based materials have achieved extremely high capacity, especially for phosphorus with a theoretical capacity of  $\sim 2600 \text{ mA h g}^{-1}$ , while the volume expansion during sodiation/desodiation is quite huge, which cannot meet the standard of commercialized cell (volume change less than

30 %). Therefore, the important research field is to design micro/nano structure or introduce a second phase as buffer matrix to improve the electrochemistry performance. Now, the universal synthesis of phosphorus is ball-milling and their properties were limited. The technical difficulty is to prepare nanosized phosphorus. Though the performance of metal oxides (such as Co-, Fe-) in a Li cell is quite outstanding, the sodium storage performance is far from satisfaction with low capacity and inferior cyclability. In addition, they also suffer from low initial coulombic efficiency and large potential hysteresis. They need to be further studied, particularly for Fe- and Mn- materials due to their extraordinary natural abundance. Though the capacity is a little low, titanium-based compounds characterized with low-strain, which is of vital importance for realizing ultra long cycling life. They make great progress with the observation of "zero-strain" P2-type layered  $\text{Na}_{0.66}[\text{Li}_{0.22}\text{Ti}_{0.78}]\text{O}_2$ . It exhibits excellent cycling stability and high rate-capability. So, titanium-based compounds seem to be promising anode for practical application. In addition, organic composites with plentiful sources and good Na storage property, are also attractive anodes for NIBs. At present, the research about organic composites is relative few and need to be further strengthened. It should be noted that most of anode materials troubled with low initial coulombic efficiency because of the irreversible formation of SEI layers. Thus, further in-depth understanding of the reaction between electrode/electrolyte must be gained. Moreover, an optimized electrolyte system (such as, with electrolyte additive FEC) which can inhibit the decomposition of electrolyte and stabilize the SEI layers, is also fatal for enhancing the electrochemical performance of materials. Above all, most researches focus on the choice and synthesis of anode materials, few researches relate to the electrochemical Na-storage mechanism, which will pave the way for designing high performance anode materials. Therefore, more attention should be paid to the electrochemistry reaction mechanism.

Similar to LIBs, NIBs also suffer from safety hazard because of the usage of organic electrolyte. The development of solid-state electrolyte is a significant aspect to address the security issues. Furthermore, aqueous Na-ion batteries, with the advantages of safety and low cost, are another new study direction.

All in all, there are still many tough challenges for the commercialization of Na-ion batteries, however, persistent efforts on exploring Na storage mechanism and failure mechanism, then designing tailored electrode materials, would make Na-ion batteries a promising alternative to LIBs for low cost, environmentally friendly, and large-scale energy storage system in the future.

## Acknowledgements

This work was financially supported by the National Natural Science Foundation of China (51231003), the Ministry of Education of China (IRT-13R30 and IRT-13022), and the 111 Project (B12015).

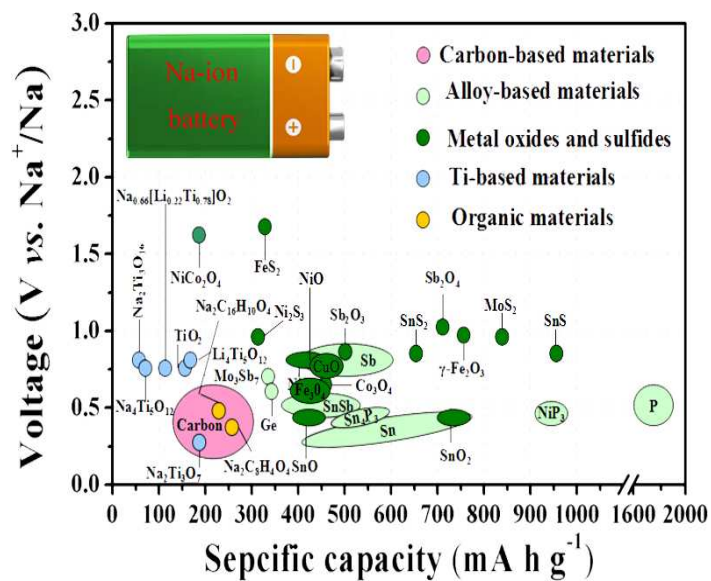
## Notes and references

- B. Dunn, H. Kamath, J. M. Tarascon, *Science*, 2011, **334**, 928-935.
- Z. G. Yang, J. L. Zhang, M. C. W. Kintner-Meyer, X. C. Lu, D. Choi, J. P. Lemmon and J. Liu, *Chem. Rev.*, 2011, **111**, 3577-3613.
- H. L. Pan, Y.-S. Hu and L. Q. Chen, *Energy Environ. Sci.*, 2013, **6**, 2338-2360.
- D. Larcher and J.-M. Tarascon, *Nat. Chem.*, 2015, **7**, 19-29.
- M. Armand and J. M. Tarascon, *Nature*, 2008, **451**, 652-657.
- M. D. Slate, D. Kim, E. Lee and C. S. Johnson, *Adv. Funct. Mater.*, 2013, **23**, 947-958.
- N. Yabuuchi, K. Kubota, M. Dahbi and S. Komaba, *Chem. Rev.*, 2014, **114**, 11636-11682.
- S. P. Ong, V. L. Chevrier, G. Hautier, A. Jain, C. Moore, S. Kim, X. H. Ma and G. Ceder, *Energy Environ. Sci.*, 2011, **4**, 3680-3688.
- V. Palomares, P. Serras, I. Villaluenga, K. B. Hueso, J. Carretero-González and T. Rojo, *Energy Environ. Sci.*, 2012, **5**, 5884-5901.
- S. Y. Hong, Y. Kim, Y. Park, A. Choi, N.-S. Choi and K. T. Lee, *Energy Environ. Sci.*, 2013, **6**, 2067-2081.
- S.-W. Kim, D.-H. Seo, X. H. Ma, G. Ceder and K. Kang, *Adv. Energy Mater.*, 2012, **2**, 710-721.
- M. M. Doeff, Y. P. Ma, S. J. Visco, L. C. Dejonghe, *J. Electrochem. Soc.*, 1993, **140**, L169-L170.
- V. L. Chevrier and G. Ceder, *J. Electrochem. Soc.*, 2011, **158**, A1011-A1014.
- G. H. Newman and L. P. Klemann, *J. Electrochem. Soc.*, 1980, **127**, 2097-2099.
- D. A. Stevens and J. R. Dahn, *J. Electrochem. Soc.*, 2000, **147**, 1271-1273.
- D. A. Stevens and J. R. Dahn, *J. Electrochem. Soc.*, 2001, **148**, A803-A811.
- V. Palomares, M. Casas-Cabanas, E. Castillo-Martínez, M. H. Han and T. Rojo, *Energy Environ. Sci.*, 2013, **6**, 2312-2337.
- Y. Kim, K.-H. Ha, S. M. Oh and K. T. Lee, *Chem. Eur. J.*, 2014, **20**, 11980-11992.
- D. Kundu, E. Talaie, V. Duffort and L. F. Nazar, *Angew. Chem. Int. Ed.*, 2015, **54**, 3431-3448.
- Y. Wen, K. He, Y. J. Zhu, F. D. Han, Y. H. Xu, I. Matsuda, Y. Ishii, J. Cumings and C. S. Wang, *Nat. Commun.*, 2014, **5**, 4033.
- Y. X. Wang, S. L. Chou, H. K. Liu, S. X. Dou, *Carbon*, 2013, **57**, 202-208.
- A. Y. Yan, Y. X. Yin, Y. G. Guo and L. J. Wan, *Adv. Energy Mater.*, 2014, **4**, 1301584.
- J. T. Xu, M. Wang, N. P. Wickramaratne, M. Jaroniec, S. X. Dou and L. M. Dai, *Adv. Mater.*, 2015, **27**, 2042-2048.
- C. Ling and F. Mizuno, *Phys. Chem. Chem. Phys.*, 2014, **16**, 10419-10424.
- R. S. Babu and M. Pyo, *J. Electrochem. Soc.*, 2014, **161**, A1045-A1050.
- K.-L. Hong, L. Qie, R. Zeng, Z.-Q. Yi, W. Zhang, D. Wang, W. Yin, C. Wu, Q.-J. Fan, W.-X. Zhang and Y.-H. Huang, *J. Mater. Chem. A*, 2014, **2**, 12733-12738.
- T. Q. Chen, Y. Liu, L. K. Pan, T. Lu, Y. F. Yao, Z. Sun, D. H. C. Chua and Q. Chen, *J. Mater. Chem. A*, 2014, **2**, 4117-4121.
- X. S. Zhou and Y. G. Guo, *ChemElectroChem*, 2014, **1**, 83-86.
- K. Gotoh, T. Ishikawa, S. Shimadzu, N. Yabuuchi, S. Komaba, K. Takeda, A. Goto, K. Deguchi, S. Ohki, K. Hashi, T. Shimizu and H. Ishida, *J. Power Sources*, 2013, **225**, 137-140.
- J. Ding, H. L. Wang, Z. Li, A. Kohandehghan, K. Cui, Z. W. Xu, B. Zahir, X. H. Tan, E. M. Lotfabad, B. C. Olsen and D. Mitlin, *ACS Nano*, 2013, **7**, 11004-11015.

- 31 K. Tang, L. J. Fu, R. J. White, L. H. Yu, M.-M. Titirici, M. Antonietti and J. Maier, *Adv. Energy Mater.*, 2012, **2**, 873-877.
- 32 Y. L. Cao, L. F. Xiao, M. L. Sushko, W. Wang, B. Schwenzer, J. Xiao, Z. M. Nie, L. V. Saraf, Z. G. Yang and J. Liu, *Nano Lett.*, 2012, **12**, 3783-3787.
- 33 Z. H. Wang, L. Qie, L. X. Yuan, W. X. Zhang, X. L. Hu and Y. H. Huang, *Carbon*, 2013, **55**, 328-334.
- 34 Y. Liu, F. F. Fan, J. W. Wang, Y. Liu, H. L. Chen, K. L. Jungjohann, Y. H. Xu, Y. J. Zhu, D. Bigio, T. Zhu and C. S. Wang, *Nano Lett.*, 2014, **14**, 3445-3452.
- 35 S. A. Webb, L. Baggetto, C. A. Bridges and G. M. Veith, *J. Power Sources*, 2014, **248**, 1105-1117.
- 36 J. W. Wang, X. H. Liu, S. X. Mao and J. Y. Huang, *Nano Lett.*, 2012, **12**, 5897-5902.
- 37 Y. C. Liu, N. Zhang, L. F. Jiao, Z. L. Tao and J. Chen, *Adv. Funct. Mater.*, 2015, **25**, 214-220.
- 38 A. Darwiche, C. Marino, M. T. Sougrati, B. Fraisse, L. Stievano and L. Monconduit, *J. Am. Chem. Soc.*, 2012, **134**, 20805-20811.
- 39 L. Baggetto, J. K. Keum, J. F. Browning and G. M. Veith, *Electrochem. Commun.*, 2013, **34**, 41-44.
- 40 J. F. Qian, X. Y. Wu, Y. L. Cao, X. P. Ai and H. X. Yang, *Angew. Chem. Int. Ed.*, 2013, **52**, 4633-4636.
- 41 Y. Kim, Y. Park, A. Choi, N. S. Choi, J. Kim, J. Lee, J. M. Ryu and K. T. Lee, *Adv. Mater.*, 2013, **25**, 3045-3049.
- 42 D. H. Nam, T.-H. Kim, K. S. Hong and H.-S. Kwon, *ACS Nano*, 2014, **8**, 11824-11835.
- 43 M. He, K. Kravchyk, M. Walter and M. V. Kovalenko, *Nano Lett.*, 2014, **14**, 1255-1262.
- 44 P. R. Abel, Y.-M. Lin, T. D. Souza, C.-Y. Chou, A. Gupta, J. B. Goodenough, G. S. Hwang, A. Heller and C. B. Mullins, *J. Phys. Chem. C*, 2013, **117**, 18885-18890.
- 45 Y. H. Xu, Y. J. Zhu, Y. H. Liu and C. S. Wang, *Adv. Energy Mater.*, 2013, **3**, 128-133.
- 46 Y. H. Liu, Y. H. Xu, Y. J. Zhu, J. N. Culver, C. A. Lundgren, K. Xu, and C. S. Wang, *ACS Nano*, 2013, **7**, 3627-3634.
- 47 Y. J. Zhu, X. G. Han, Y. H. Xu, Y. H. Liu, S. Y. Zheng, K. Xu, L. B. Hu and C. S. Wang, *ACS Nano*, 2013, **7**, 6378-6386.
- 48 Y. N. Ko and Y. C. Kang, *Chem. Commun.*, 2014, **50**, 12322-12324.
- 49 L. Wu, H. Y. Lu, L. F. Xiao, X. P. Ai, H. X. Yang and Y. L. Cao, *J. Mater. Chem. A*, 2015, **3**, 5708-5713.
- 50 L. Wu, X. H. Hu, J. F. Qian, F. Pei, F. Y. Wu, R. J. Mao, X. P. Ai, H. X. Yang and Y. L. Cao, *Energy Environ. Sci.*, 2014, **7**, 323-328.
- 51 L. Fan, J. J. Zhang, J. H. Cui, Y. C. Zhu, J. W. Liang, L. L. Wang and Y. T. Qian, *J. Mater. Chem. A*, 2015, **3**, 3276-3280.
- 52 Y. J. Zhu, Y. Wen, X. L. Fan, T. Gao, F. D. Han, C. Luo, S. C. Liou and C. S. Wang, *ACS Nano*, 2015, **9**, 3254-3264.
- 53 J. X. Song, Z. X. Yu, M. L. Gordin, S. Hu, R. Yi, D. H. Tang, T. Walter, M. Regula, D. Choi, X. L. Li, A. Manivannan and D. H. Wang, *Nano Lett.*, 2014, **14**, 6329-6335.
- 54 T. Ramireddy, T. Xing, M. M. Rahman, Y. Chen, Q. Dutercq, D. Gunzelmann and A. M. Glushenkov, *J. Mater. Chem. A*, 2015, **3**, 5572-5584.
- 55 Y.-M. Lin, P. R. Abel, A. Gupta, J. B. Goodenough, A. Heller and C. B. Mullins, *ACS Appl. Mater. Interfaces*, 2013, **5**, 8273-8277.
- 56 J. Liu, Y. R. Wen, P. A. van Aken, J. Maier and Y. Yu, *Nano Lett.*, 2014, **14**, 6387-6392.
- 57 Y. Yui, Y. Ono, M. Hayashi, Y. Nemoto, K. Hayashi, K. Asakura and H. Kitabayashi, *J. Electrochem. Soc.*, 2015, **162**, A3098-A3102.
- 58 L. Baggetto, M. Marszewski, J. Górka, M. Jaroniec and G. M. Veith, *J. Power Sources*, 2013, **243**, 699-705.
- 59 D.-H. Nam, K.-S. Hong, S.-J. Lim and H.-S. Kwon, *J. Power Sources*, 2014, **247**, 423-427.
- 60 E. D. Jackson, S. Green, and A. L. Prieto, *ACS Appl. Mater. Interfaces*, 2015, **7**, 7447-7450.
- 61 L. Baggetto, E. Allcorn, R. R. Unocic, A. Manthiram and G. M. Veith, *J. Mater. Chem. A*, 2013, **1**, 11163-11169.
- 62 Y. B. Zhao and A. Manthiram, *Chem. Mater.*, 2015, **27**, 3096-3101.
- 63 J. Fullenwarth, A. Darwiche, A. Soares, B. Donnadieu and L. Monconduit, *J. Mater. Chem. A*, 2014, **2**, 2050-2059.
- 64 W. J. Li, S. L. Chou, J. Z. Wang, H. K. Liu and S. X. Dou, *Chem. Commun.*, 2015, **51**, 3682-3685.
- 65 L. F. Xiao, Y. L. Cao, J. Xiao, W. Wang, L. Kovarik, Z. Niewa and J. Liu, *Chem. Commun.*, 2012, **48**, 3321-3323.
- 66 L. Baggetto, H.-Y. Hah, J.-C. Jumas, C. E. Johnson, J. A. Johnson, J. K. Keum, C. A. Bridges, G. M. Veith, *J. Power Sources*, 2014, **267**, 329-336.
- 67 L. Li, K. H. Seng, D. Li, Y. Y. Xia, H. K. Liu and Z. P. Guo, *Nano Res.*, 2014, **7**, 1466-1476.
- 68 Y. Kim, Y. Kim, A. Choi, S. Woo, D. Mok, N.-S. Choi, Y. S. Jung, J. H. Ryu, S. M. Oh and K. T. Lee, *Adv. Mater.*, 2014, **26**, 4139-4144.
- 69 J. F. Qian, Y. Xiong, Y. L. Cao, X. P. Ai and H. X. Yang, *Nano Lett.*, 2014, **14**, 1865-1869.
- 70 W. J. Li, S. L. Chou, J. Z. Wang, J. H. Kim, H. K. Liu and S. X. Dou, *Adv. Mater.*, 2014, **26**, 4037-4042.
- 71 B. Farbod, K. Cui, W. P. Kalisvaart, M. Kupsta, B. Zahiri, A. Kohandehghan, E. M. Lotfabad, Z. Li, E. J. Lubber and D. Mitlin, *ACS Nano*, 2014, **8**, 4415-4429.
- 72 S. Komaba, Y. Matsuura, T. Ishikawa, N. Yabuuchi, W. Murata and S. Kuze, *Electrochem. Commun.*, 2012, **21**, 65-68.
- 73 L. W. Ji, M. Gu, Y. Y. Shao, X. L. Li, M. H. Engelhard, B. W. Arey, W. Wang, Z. M. Nie, J. Xiao, C. M. Wang, J. G. Zhang and J. Liu, *Adv. Mater.*, 2014, **26**, 2901-2908.
- 74 J. Y. Jang, Y. Lee, Y. Kim, J. Lee, S.-M. Lee, K. T. Lee and N.-S. Choi, *J. Mater. Chem. A*, 2015, **3**, 8332-8338.
- 75 L. J. Wang, K. Zhang, Z. Hu, W. C. Duan, F. Y. Cheng and J. Chen, *Nano Res.*, 2014, **7**, 199-208.
- 76 S. Yuan, X. L. Huang, D. L. Ma, H. G. Wang, F. Z. Meng and X. B. Zhang, *Adv. Mater.*, 2014, **26**, 2273-2279.
- 77 M. M. Rahman, A. M. Glushenkov, T. Ramireddy and Y. Chen, *Chem. Commun.*, 2014, **50**, 5057-5060.
- 78 Z. L. Jian, B. Zhao, P. Liu, F. J. Li, M. B. Zheng, M. W. Chen, Y. Shi and H. S. Zhou, *Chem. Commun.*, 2014, **50**, 1215-1217.
- 79 N. Zhang, X. P. Han, Y. C. Liu, X. F. Hu, Q. Zhao and J. Chen, *Adv. Energy Mater.*, 2015, **5**, 1401123.
- 80 Y. Y. Lu, N. Zhang, Q. Zhao, J. Liang and J. Chen, *Nanoscale*, 2015, **7**, 2770-2776.
- 81 Y. Zhao, Z. X. Feng and Z. C. J. Xu, *Nanoscale*, 2015, **7**, 9520-9525.
- 82 R. Alca'ntara, M. Jaraba, P. Lavela, and J. L. Tirado, *Chem. Mater.*, 2002, **14**, 2847-2848.
- 83 S. Komaba, T. Mikumo, N. Yabuuchi, A. Ogata, H. Yoshida and Y. Yamada, *J. Electrochem. Soc.*, 2010, **157**, A60-A65.
- 84 S. M. Oh, S. T. Myung, C. S. Yoon, J. Lu, J. Hassoun, B. Scrosati, K. Amine and Y.-K. Sun, *Nano Lett.*, 2014, **14**, 1620-1626.
- 85 J. W. Wen, D. W. Zhang, Y. Zang, X. Sun, B. Cheng, C. X. Ding, Y. Yu, C. H. Chen, *Electrochim. Acta*, 2014, **132**, 193-199.
- 86 Y. G. Liu, Z. Y. Cheng, H. Y. Sun, H. Arandiyani, J. P. Li and M. Ahmad, *J. Power Sources*, 2015, **273**, 878-884.
- 87 M. C. López, P. Lavela, G. F. Ortiz and J. L. Tirado, *Electrochem. Commun.*, 2013, **27**, 152-155.
- 88 W. P. Sun, X. H. Rui, J. X. Zhu, L. H. Yu, Y. Zhang, Z. C. Xu, S. Madhavi and Q. Y. Yan, *J. Power Sources*, 2015, **274**, 755-761.
- 89 S. Hariharan, K. Saravanan and P. Balaya, *Electrochem. Commun.*, 2013, **31**, 5-9.

- 90 Y. Liu, B. H. Zhang, S. Y. Xiao, L. L. Liu, Z. B. Wen and Y. P. Wu, *Electrochim. Acta*, 2014, **116**, 512-517.
- 91 Y. Z. Jiang, M. J. Hu, D. Zhang, T. Z. Yuan, W. P. Sun, B. Xu and M. Yan, *Nano Energy*, 2014, **5**, 60-66.
- 92 J. Ming, H. Ming, W.-J. Kwak, C. Shin, J. W. Zheng and Y.-K. Sun, *Chem. Commun.*, 2014, **50**, 13307-13310.
- 93 D. W. Su, X. Q. Xie, and G. X. Wang, *Chem. Eur. J.*, 2014, **20**, 3192-3197.
- 94 L. K. Pei, Q. Jin, Z. Q. Zhu, Q. Zhao, J. Liang and Jun Chen, *Nano Res.*, 2015, **8**, 184-192.
- 95 D. W. Su, H. J. Ahn and G. X. Wang, *Chem. Commun.*, 2013, **49**, 3131-3133.
- 96 J. Ding, Z. Li, H. L. Wang, K. Cui, A. Kohandehghan, X. H. Tan, D. Karpuzov and D. Mitlin, *J. Mater. Chem. A*, 2015, **3**, 7100-7111.
- 97 D. W. Su, C. Y. Wang, H. J. Ahn and G. X. Wang, *Phys. Chem. Chem. Phys.*, 2013, **15**, 12543-12550.
- 98 Y. X. Wang, Y. G. Lim, M. S. Park, S. L. Chou, J. H. Kim, H. K. Liu, S. K. Dou and Y. J. Kim *J. Mater. Chem. A*, 2014, **2**, 529-534.
- 99 X. Q. Xie, D. W. Su, J. Q. Zhang, S. Q. Chen, A. K. Mondal and G. X. Wang, *Nanoscale*, 2015, **7**, 3164-3172.
- 100 M. Shimizu, H. Usui and H. Sakaguchi, *J. Power Sources*, 2014, **248**, 378-382.
- 101 M. Gu, A. Kushima, Y. Y. Shao, J. G. Zhang, J. Liu, N. D. Browning, J. Li and C. M. Wang, *Nano Lett.*, 2013, **13**, 5203-5211.
- 102 N. Li, S. Liao, Y. Sun, H. W. Song and C. X. Wang, *J. Mater. Chem. A*, 2015, **3**, 5820-5828.
- 103 X. S. Zhou, X. Liu, Y. Xu, Y. X. Liu, Z. H. Dai and J. C. Bao, *J. Phys. Chem. C*, 2014, **118**, 23527-23534.
- 104 Q. Sun, Q. Q. Ren, H. Li and Z. W. Fu, *Electrochem. Commun.*, 2011, **13**, 1462-1464.
- 105 X. F. Wang, X. Shen, Z. X. Wang, R. C. Yu and L. Q. Chen, *ACS Nano*, 2014, **8**, 11394-11400.
- 106 C. B. Zhu, X. K. Mu, P. A. van. Aken, Y. Yu and J. Maier, *Angew. Chem. Int. Ed.*, 2014, **53**, 2152-2156.
- 107 Z. Hu, L. X. Wang, K. Zhang, J. B. Wang, F. Y. Cheng, Z. L. Tao and J. Chen, *Angew. Chem. Int. Ed.*, 2014, **53**, 12794-12798.
- 108 Z. Hu, Z. Q. Zhu, F. Y. Cheng, K. Zhang, J. B. Wang, C. C. Chen and J. Chen, *Energy Environ. Sci.*, 2015, **8**, 1309-1316.
- 109 J. Park, J.-S. Kim, J.-W. Park, T.-H. Nam, K.-W. Kim, J.-H. Ahn, G. X. Wang and H.-J. Ahn, *Electrochim. Acta*, 2013, **92**, 427-432.
- 110 L. David, R. Bhandavat and G. Singh, *ACS Nano*, 2014, **8**, 1759-1770.
- 111 Y. X. Wang, K. H. Seng, S. L. Chou, J. Z. Wang, Z. P. Guo, D. Wexler, H. K. Liu and S. X. Dou, *Chem. Commun.*, 2014, **50**, 10730-10733.
- 112 S. H. Choi, Y. N. Ko, J.-K. Lee and Y. C. Kang, *Adv. Funct. Mater.*, 2015, **25**, 201402428.
- 113 J. J. Wang, C. Luo, T. Gao, A. Langrock, A. C. Mignerey and C. S. Wang, *Small*, 2015, **11**, 473-481.
- 114 X. Q. Xiong, W. Luo, X. L. Hu, C. J. Chen, L. Qie, D. F. Hou and Y. H. Huang, *Sci. Rep.*, 2015, **5**, 9254.
- 115 X. Q. Xie, Z. Ao, D. W. Su, J. Q. Zhang and G. X. Wang, *Adv. Funct. Mater.*, 2015, **25**, 1393-1403.
- 116 S. D. Lacey, J. Y. Wan, A. W. Cresce, S. M. Russell, J. Q. Dai, W. Z. Bao, K. Xu and L.B. Hu, *Nano Lett.*, 2015, **15**, 1018-1024.
- 117 Y. C. Liu, H. Y. Kang, L. F. Jiao, C. C. Chen, K. Z. Cao, Y. J. Wang and H. T. Yuan, *Nanoscale*, 2015, **7**, 1325-1332.
- 118 Y. D. Zhang, P. Y. Zhu, L. L. Huang, J. Xie, S. C. Zhang, G. S. Cao and X. B. Zhao, *Adv. Funct. Mater.*, 2015, **25**, 481-489.
- 119 B. H. Qu, C. Z. Ma, G. Ji, C. H. Xu, J. Xu, Y. S. Meng, T. H. Wang and J. Y. Lee, *Adv. Mater.*, 2014, **26**, 3854-3859.
- 120 T. F. Zhou, W. K. Pang, C. F. Zhang, J. P. Yang, Z. X. Chen, H. K. Liu and Z. P. Guo, *ACS Nano*, 2014, **8**, 8323-8333.
- 121 S. H. Choi and Y. C. Kang, *Nano Res.*, 2015, **8**, 1595-1603.
- 122 D. W. Su, S. X. Dou and G. X. Wang, *Chem. Commun.*, 2014, **50**, 4192-4195.
- 123 S. H. Choi and Y. C. Kang, *Nanoscale*, 2015, **7**, 3965-3970.
- 124 H. S. Ryu, J. S. Kim, J. S. Park, J. W. Park, K. W. Kim, J. H. Ahn, T. H. Nam, G. X. Wang and H. J. Ahn, *J. Electrochem. Soc.*, 2013, **160**, A338-A343.
- 125 M. W. T. Zünd and M. V. Kovalenko, *Nanoscale*, 2015, **7**, 9158-9163.
- 126 S. S. Zhang, *J. Mater. Chem. A*, 2015, **3**, 7689-7694.
- 127 Y. Y. Zhu, P. Nie, L. F. Shen, S. Y. Dong, Q. Sheng, H. S. Li, H. F. Luo, X. G. Zhang, *Nanoscale*, 2015, **7**, 3309-3315.
- 128 C. Q. Shang, S. M. Dong, S. L. Zhan, P. Hu, C. J. Zhang, G. L. Cui, *Electrochem. Commun.*, 2015, **50**, 24-27.
- 129 T. B. Kim, J. W. Choi, H. S. Ryu, G. B. Cho, K. W. Kim, J. H. Ahn, K. K. Cho and H. J. Ahn, *J. Power Sources*, 2007, **174**, 1275-1278.
- 130 H. L. Pan, X. Lu, X. Q. Yu, Y.-S. Hu, H. Li, X.-Q. Yang and L. Q. Chen, *Adv. Energy Mater.*, 2013, **3**, 1186-1194.
- 131 Y. Sun, L. Zhao, H. L. Pan, X. Lu, L. Gu, Y. S. Hu, H. Li, M. Armand, Y. Ikuhara, L. Q. Chen and X. J. Huang, *Nat. Commun.*, 2013, **4**, 1870.
- 132 B.-R. Lee and E.-S. Oh, *J. Phys. Chem. C*, 2013, **117**, 4404-4409.
- 133 L. M. Wu, D. Buchholz, D. Bresser, L. G. Chagas and S. Passerini, *J. Power Sources*, 2014, **251**, 379-385.
- 134 K.-T. Kim, G. Ali, K. Y. Chung, C. S. Yoon, H. Yashiro, Y.-K. Sun, J. Lu, K. Amine and S.-T. Myung, *Nano Lett.*, 2014, **14**, 416-422.
- 135 Y. Xu, E. M. Lotfabad, H. L. Wang, B. Farbod, Z. W. Xu, A. Kohandehghan and D. Mitlin, *Chem. Commun.*, 2013, **49**, 8973-8975.
- 136 H. A. Cha, H. M. Jeong and J. K. Kang, *J. Mater. Chem. A*, 2014, **2**, 5182-5186.
- 137 L. M. Wu, D. Bresser, D. Buchholz, G. A. Giffin, C. R. Castro, A. Ochel and S. Passerini, *Adv. Energy Mater.*, 2015, **5**, 1401142.
- 138 J. P. Huang, D. D. Yuan, H. Z. Zhang, Y. L. Cao, G. R. Li, H. X. Yang and X. P. Gao, *RSC Adv.*, 2013, **3**, 12593-12597.
- 139 J. C. Pérez-Flores, C. Baehtz, A. Kuhn and F. García-Alvarado, *J. Mater. Chem. A*, 2014, **2**, 1825-1833.
- 140 Y. C. Yang, X. B. Ji, M. J. Jing, H. S. Hou, Y. R. Zhu, L. B. Fang, X. M. Yang, Q. Y. Chen and C. E. Banks, *J. Mater. Chem. A*, 2015, **3**, 5648-5655.
- 141 H. Usui, S. Yoshioka, K. Wasada, M. Shimizu and H. Sakaguchi, *ACS Appl. Mater. Interfaces*, 2015, **7**, 6567-6573.
- 142 D. Yan, C. Y. Yu, Y. Bai, W. F. Zhang, T. Q. Chen, B. W. Hu, Z. Sun and L. K. Pan, *Chem. Commun.*, 2015, **51**, 8261-8264.
- 143 J. R. González, R. Alcántara, F. Nacimiento, G. F. Ortiz and J. L. Tirado, *CrystEngComm*, 2014, **16**, 4602-4609.
- 144 C. J. Chen, Y. W. Wen, X. L. Hu, X. L. Ji, M. Y. Yan, L. Q. Mai, P. Hu, B. Shan and Y. H. Huang, *Nat. Commun.*, 2015, **6**, doi:10.1038/ncomms7929.
- 145 L. Zhao, H. L. Pan, Y. S. Hu, H. Li and L. Q. Chen, *Chin. Phys. B*, 2012, **21**, 028201.
- 146 X. Q. Yu, H. L. Pan, W. Wan, C. Ma, J. M. Bai, Q. P. Meng, S. N. Ehrlich, Y. S. Hu and X. Q. Yang, *Nano Lett.*, 2013, **13**, 4721-4727.
- 147 G. Hasegawa, K. Kanamori, T. Kiyomura, H. Kurata, K. Nakanishi and T. Abe, *Adv. Energy Mater.*, 2015, **5**, 1400730.
- 148 P. F. Yu, C. L. Li and X. X. Guo, *J. Phys. Chem. C*, 2014, **118**, 10616-10624.
- 149 P. J. P. Naeyaert, M. Avdeev, N. Sharma, H. B. Yahia and C. D. Ling, *Chem. Mater.*, 2014, **26**, 7067-7072.
- 150 P. Senguttuvan, G. Rousse, V. Seznec, J.-M. Tarascon and M. R. Palacin, *Chem. Mater.*, 2011, **23**, 4109-4111.
- 151 H. L. Pan, X. Lu, X. Q. Yu, Y.-S. Hu, H. Li, X.-Q. Yang and L. Q. Chen, *Adv. Energy Mater.*, 2013, **3**, 1186-1194.

- 152 Y. P. Zhang, L. Guo and S. H. Yang, *Chem. Commun.*, 2014, **50**, 14029-14032.
- 153 J. Xu, C. Z. Ma, M. Balasubramanian and Y. S. Meng, *Chem. Commun.*, 2014, **50**, 12564-12567.
- 154 A. Rudola, K. Saravanan, C. W. Masona and P. Balaya, *J. Mater. Chem. A*, 2013, **1**, 2653-2662.
- 155 A. Rudola, K. Saravanan, S. Devaraj, H. Gong and P. Balaya, *Chem. Commun.*, 2013, **49**, 7451-7453.
- 156 K. Shen and M. Wagemaker, *Inorg. Chem.*, 2014, **53**, 8250-8256.
- 157 Y. S. Wang, X. Q. Yu, S. Y. Xu, J. M. Bai, R. J. Xiao, Y. S. Hu, H. Li, X. Q. Yang, L. Q. Chen and X. J. Huang, *Nat. Commun.*, 2013, **4**, 2365.
- 158 M. Shirpour, J. Cabana and M. Doeff, *Energy Environ. Sci.*, 2013, **6**, 2538-2547.
- 159 D. Seshadri, M. Shirpour and M. Doeff, *J. Electrochem. Soc.*, 2015, **162**, A52-A59.
- 160 F. X. Xie, Y. F. Deng, Y. Xie, H. J. Xud and G. H. Chen, *Chem. Commun.*, 2015, **51**, 3545-3548.
- 161 J.-P. Bonnet, S. Renault, F. Dolhem, P. Poizot, *Energy Environ. Sci.*, 2010, **3**, 1929-1933.
- 162 L. Zhao, J. M. Zhao, Y. S. Hu, H. Li, Z. B. Zhou, M. Armand and L. Q. Chen, *Adv. Energy Mater.*, 2012, **2**, 962-965.
- 163 Y. Park, D.-S. Shin, S. H. Woo, N. S. Choi, K. H. Shin, S. M. Oh, K. T. Lee and S. Y. Hong, *Adv. Mater.*, 2012, **24**, 3562-3567.
- 164 Z. Q. Zhu, H. Li, J. Liang, Z. L. Tao and J. Chen, *Chem. Commun.*, 2015, **51**, 1446-1448.
- 165 D. J. Kim, Y. H. Jung, K. K. Bharathi, S. H. Je, D. K. Kim, A. Coskun and J. W. Choi, *Adv. Energy Mater.*, 2014, **4**, 1400133.
- 166 C. L. Wang, Y. Xu, Y. G. Fang, M. Zhou, L. Y. Liang, S. Singh, H. P. Zhao, A. Schober and Y. Lei, *J. Am. Chem. Soc.*, 2015, **137**, 3124-3130.
- 167 A. Choi, Y. K. Kim, T. K. Kim, M.-S. Kwon, K. T. Lee and H. R. Moon, *J. Mater. Chem. A*, 2014, **2**, 14986-14993.
- 168 S. W. Wang, L. J. Wang, Z. Q. Zhu, Z. Hu, Q. Zhao and J. Chen, *Angew. Chem. Int. Ed.*, 2014, **53**, 5892-5896.
- 169 E. Castillo-Martínez, J. Carretero-González and M. Armand, *Angew. Chem. Int. Ed.*, 2014, **53**, 5341-5345.



This review is focused on the recent progress and strategies in fabricating high performance anode materials for Na-ion batteries.